ACS Sustainable Chemistry & Engineering

pubs.acs.org/journal/ascecg

Research Article

Atomic-Scale Charge Distribution Mapping of Single Substitutional p- and n-Type Dopants in Graphene

Benjamin Mallada, Shayan Edalatmanesh, Petr Lazar, Jesus Redondo, Aurelio Gallardo, Radek Zbořil, Pavel Jelínek,* Martin Švec,* and Bruno de la Torre*

Cite This: *ACS Sustainable Chem. Eng.* 2020, 8, 3437−3444

Read Online

ACCESS | Metrics & More | Article Recommendations | Supporting Information

ABSTRACT: Tuning the chemical properties of graphene by controlled doping is a widely investigated strategy. The effect of a substitutional single dopant on graphene local reactivity is much less explored. To improve the understanding of the role of p- and n-type dopants in graphene's local chemical activity and quantification of its interaction with single molecules, we report an atomic-scale investigation of single boron (B) and nitrogen (N) dopants in graphene and their interactions with CO molecules by means of atomic force microscopy (AFM) and Kelvin probe force microscopy (KPFM) experiments and theoretical calculations. We infer that N/B doping significantly increases/lowers the chemical interaction of graphene with individual CO molecules as a result of weak electrostatic forces induced by distinct charge distribution around the dopant site. High-resolution AFM images allow dopant discrimination and their atomic-scale structural characterization, which may be crucial for the atomic-scale design of graphene derivatives with relevant potential applications in molecular sensing and catalysis.

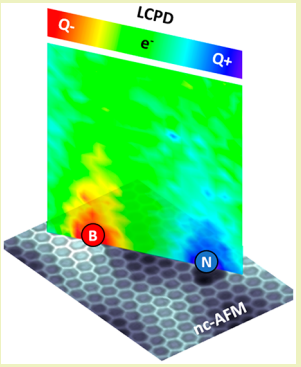

KEYWORDS: *Graphene, Nitrogen doping, Boron doping, Graphene chemistry, Noncovalent interactions, CO−graphene interaction, Scanning probe microscopy, Density functional theory*

INTRODUCTION

The fundamental understanding of the physical and chemical properties of individual dopants incorporated in graphene is crucial for a successful application in graphene-based devices. Doping with heteroatoms has become one of the most successful routes for addressing desirable functionalities in graphene. In particular, incorporation of substitutional boron and nitrogen atoms in the graphene lattice creates acceptor and donor centers, due to the different number of valence electrons with respect to carbon.[1−4] The size and electronic structure similar to carbon provide them with specific advantages for their substitution into the graphene sheet with minimal strain, maintaining the overall graphene structure. Such dopants affect graphene charge transport[5,6] and plasmon mobility[7] and induce magnetism.[6,8] Great efforts have also been dedicated to address their specific chemical functionalities.[9,10] Due to the inertness of the pristine graphene, incorporation of atomic and molecular species in the two-dimensional lattice provides enhanced chemical activity of doped graphene, offering a multitude of applications.[11]

Recent investigation of nitrogen- and boron-doped graphene derivatives[12−16] has been focused on the dopant physicochemical properties at the atomic level. A comprehensive experimental structure elucidation and charge distribution of the N- and B-doped carbon sheet at the atomic scale are still missing. It is worth mentioning that numerous theoretical studies addressing the electronic and chemical properties of the dopant sites reported dopant charges, which differ widely in magnitude and even in sign.[17−20] A Bader charge analysis of theoretical data predicted that the N dopant gains 1.2 e^- rather than losing charge as expected for an n-type dopant.[21,22] The real charge redistribution is crucial for understanding the modification of graphene chemistry upon doping,[23,24] i.e., of the interaction of boron and nitrogen dopants with molecules and other functional moieties. The in-plane component of the dopant electrostatic force field plays a significant role in graphene charge carrier scattering,[7,25,26] while the out-of-plane component dominates the chemical interaction and may be useful for creating selective sites for graphene functionalization with organic molecules.[27−30]

Here, we report on a low-temperature noncontact atomic force microscopy (nc-AFM) and Kelvin probe force microscopy (KPFM) investigation with a functionalized CO-tip[31] of individual nitrogen and boron dopants implanted in a graphene monolayer grown on SiC(0001), complemented by theoretical calculations. We evaluate the noncovalent interactions of nitrogen and boron dopants with CO molecules attached to the apex of an AFM tip with respect to the

Received: December 20, 2019
Revised: February 5, 2020
Published: February 6, 2020

graphene substrate. We map the redistribution of electron densities at C−N and C−B bonds that accompanies the incorporation of sp^2 nitrogen and boron dopants in graphene. This gives rise to net positive and negative static charges localized a few angstroms around the nitrogen and boron sites, respectively, which determine the doped graphene chemical activity through weak electrostatic forces.

METHODS

Experimental Methods. 6H-SiC(0001) samples were cut from TankeBlue research grade wafers using a diamond scribe and PEEK tipped tweezers. The samples were degassed up to 900 °C in UHV and subsequently exposed to a Si flux for 40 min. Once a sharp 3 × 3 LEED pattern was acquired, the graphene was grown by annealing up to 1300 °C, increasing 50 °C every 5 min. Boron doping[32] was achieved by sublimating B from a commercial evaporator on the already-grown graphene at RT (a flux of 26 nA for 20 s was enough to obtain a low concentration of dopants) and a final annealing at 1150 °C for 20 min. The growth and the doping were monitored by means of LEED and STM. The temperature was controlled using a Micro-Epsilon 2MH-CF3 thermometer of a 1.6 μm spectral range with and emissivity of 0.9. N atom implantation was achieved by sputtering the graphene sample with N atoms accelerated at 120 eV and subsequent annealing to approximately 800 °C.

STM/AFM measurements were carried out in a UHV chamber equipped with a low-temperature STM/AFM with qPlus tuning fork sensor operated at 5 K (Createc GmbH). During the AFM measurements, a Pt/Ir tip mounted onto the sensor (frequency ≈ 30 kHz; stiffness ≈ 1800 N/m) was oscillated with a constant amplitude of 50 pm. To obtain high-resolution AFM/STM images, prior to the experiment, the tip was functionalized with a CO molecule gathered from a Au(111) surface. Before transfer of the CO-tip to graphene, we did several approach/retract (up to few micrometers) experiments on Au(111) to select only highly stable CO-tips for transfer to graphene. On graphene, we benchmarked CO presence at the tip apex by constant height AFM atomic-scale images at various tip-sample distances. CO-tip images lead characteristic honeycomb features of graphene whereas metallic tips display hexagonal pattern47 (see Figure S5).

For the local contact potential difference (LCPD) mapping in the XZ plane on both dopants, 1250 KPFM measurements were performed with a bias range [−500 mV, 300 mV] in a grid of size of 3 nm × 1 nm. The acquisition time for each parabola was 30 s. The mapping was generated by fitting each parabola by the formula $a(x\text{-LCPD})^2 + c$ with a Python script and assigning the fitted value of the LCPD for every (x,z) position to a 25 × 50 grid of pixels. STM/AFM images were analyzed using WSxM software.[33]

DFT Methods. Density functional theory calculations were performed using the projector-augmented wave method in the Vienna Ab initio Simulation Package (VASP).[34,35] The surface of graphene was modeled using a supercell of 5 × 5 elementary cells (50 carbon atoms). The tip was modeled by the CO molecule attached to the apex gold atom of a triangular pyramid Au cluster (10 Au atoms) having Au(111) faces. The outer layer of the Au cluster and two atoms of graphene were fixed, while the rest of the system (CO molecule and adjacent Au atoms, graphene atoms beneath the tip) was allowed to fully relax.

The 3 × 3 × 1 k-point grid was used to sample the Brillouin zone. The periodically repeated supercells were separated by 25 Å of vacuum. The energy cutoff for the plane-wave expansion was set to 400 eV. We used the optimized van der Waals functional optB86b-vdW[36] in all calculations, which provided a balanced description of van der Waals and covalent bonding in our previous studies.[37,38] We tested also the many-body dispersion method MBD+rscs and empirical dispersion DFT+D2. In order test robustness of our theoretical calculation, we used also the many-body dispersion MBD@rsSCS functional.[39] The interaction energies and their order for the tip above a C, N, B atoms were very similar to those obtained using optB86b-vdW (Figure S2). The plots of the induced charge density isosurface were prepared using VESTA software[40]

Hartree potential calculations were done by employing FHI-AIMS[41] code, using two geometrically relaxed slabs of 180 atoms with a periodic boundary condition (PBC). The systems were allowed to relax until the remaining atomic forces reached below 10^{-2} eV/Å. The GGA-PBE[42] functional was used as the exchange−correlation functional and a grid of 4 × 4 × 1 k-points to sample the Brillouin Zone.

AFM images were calculated using the probe particle model.[43] The parameters of the tip were chosen to mimic a CO-tip. Namely, charge distribution of the CO molecule was mimicked by a quadrupole moment[44] with a value of −0.1e and lateral stiffness of the probe particle of 0.25 N m^{-1}. The electrostatic interaction between the tip and the sample was included in the AFM calculations using the Hartree potential obtained from fully optimized total energy DFT calculations using the VASP code.[34] These DFT calculations were done using a 6 × 6 × 1 k-point reciprocal grid in a 7 × 7 supercell. To simulate the dynamic of the tip, we used typical values of a qPlus sensor, oscillation amplitude A = 100 pm, sensor stiffness k = 3600 N/m, and eigenfrequency f_0 = 30 kHz.

RESULTS AND DISCUSSION

Structural Characterization of B- and N-Doped Graphene. We have carried out combined low-temperature (5 K) STM/nc-AFM experiments on atomically well-defined graphene, doped with single nitrogen and boron atoms in a substitutional configuration. A graphene monolayer is grown on a SiC(0001) substrate and subsequently doped with boron and nitrogen atoms in a stepwise process in ultrahigh vacuum (see Methods for details). Both boron and nitrogen atoms were implanted in low concentrations, which facilitates the study of individual dopant sites on the surface. All the experiments were performed with an STM/AFM tip-apex functionalized with a single CO molecule picked up from a nearby Au(111) substrate.

A typical STM topography of a graphene region which comprises three nitrogen dopants and one boron dopant is shown in Figure 1a. Dopants are featured as three-fold protrusions distributed randomly on the surface with no apparent preference of incorporation in the graphene lattice. Characteristics in STM features of graphene dopants are strongly dependent on the tip termination.[4,45] We have found that functionalization of the tip with CO molecules provides a very reproducible STM contrast for several experimental

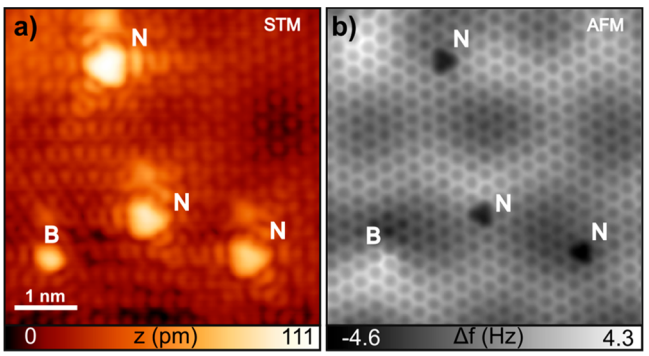

Figure 1. Graphitic boron and nitrogen dopants in graphene. STM topography (a) and constant-height nc-AFM (b) images of a graphene area with one boron and three nitrogen substitutional dopants. In nc-AFM images, boron (bottom left-hand) and nitrogen dopants are resolved as bright and dark features, respectively. STM image parameters: 200 mV, 50 pA.

https://dx.doi.org/10.1021/acssuschemeng.9b07623
ACS Sustainable Chem. Eng. 2020, 8, 3437−3444

sessions. The assignment of graphitic nitrogen and boron dopants is corroborated by constant-height high-resolution AFM imaging with a CO-tip of the same graphene area (Figure 1b). The periodic honeycomb structure of carbon atoms is clearly resolved together with the graphene moiré pattern on a larger length scale, which is the $6\sqrt{3}$x$6\sqrt{3}$-R30° quasiperiodic structure of the buffer layer and is observed in both STM and AFM images, pointing out its topographic origin. The use of a nonreactive CO-tip allows us to evaluate the true topographic corrugation[46,47] of the moiré from direct comparison of the AFM contrast at several tip−sample distances for high and low graphene areas, similarly as reported by Schwarz et al.[48] (Figure S1). With this method, we reach an estimate of 20−30 pm in good agreement with previous room-temperature AFM[49] experiments on the same surface. Interestingly, for an adequate tip−sample height, a pronounced variation of the atomic-scale contrast is observed at the dopant sites; i.e., boron and nitrogen atoms are brighter and darker than the surrounding carbon atoms, respectively. This is observed regardless of localization of the dopants in the moiré superlattice, thus allowing us to rule out any influence of the dopant hybridization with the substrate.

Next, we focus on the contrast of boron and nitrogen dopants in AFM images. Figure 2 shows a series of detailed experimental AFM images of boron (top) and nitrogen (bottom) in graphene as a function of the tip−sample separation. Hereinafter, the closest tip−sample separation ($z_{rel.}$ = 0 pm) is referred to as a tip approach of 150 pm from STM point (−500 mV, 50 pA). At the largest separation (left-hand panel; $z_{rel.}$ = 120 pm), bright (less negative frequency shift) and dark (more negative frequency shift) features are observed at boron (red dot) and nitrogen (blue dot) sites. Upon the tip approach (centered panel; $z_{rel.}$ = 90 pm), the carbon hexagons of graphene are clearly resolved. The three C−B bonds around the boron atom are comparatively brighter than the surrounding C−C bonds. In contrast, no marks of C−N bonds are observed at the same tip−sample distance. At $z_{rel.}$ = 60 pm, all the three C−N bonds start to be resolved, while the C−B bonds appearance becomes similar to that of the C−C bonds. Interestingly, the AFM image at a close distance reveals a distortion of the carbon rings in the proximity of the dopants. Previously, similar lateral distortions were attributed to spatial variations of electrostatic potential within a molecule,[50] thus suggesting localization of electrostatic charges around dopants, as we discuss later. These characteristic contrast features in the AFM images have been observed with several different CO-tips and on dopants located at distinct moiré sites, which proves that the types of contrasts are intrinsic and unique to the doping element. Similar characteristics have been reported recently in AFM images with a CO-tip on boron- and nitrogen-doped graphene nanoribbons on Au(111)[51] and attributed to the modulated local electron density caused by the substitution. Qualitatively, we observed a C−N bond length of 188 ± 8 pm and C−B bond length of 134 ± 4 pm, which differ from the observed bond length of unperturbed C−C bonds of 141 ± 2 pm (Figure S4), in perfect agreement with similar observations in B- and N-doped nanoribbons.[51]

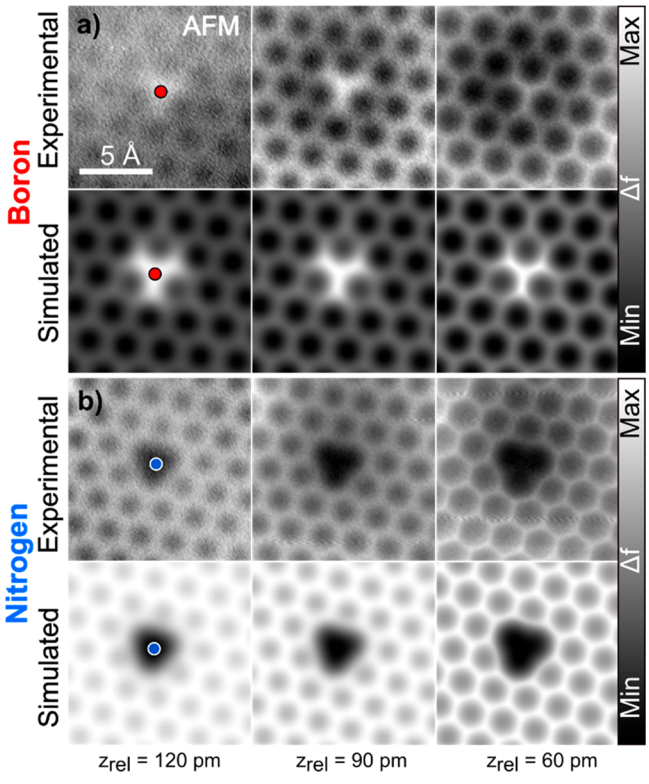

Figure 2. High-resolution AFM images on dopants with a CO-tip. Experimental (top row) and simulated (bottom row) constant-height AFM images of a single boron dopant (a) and nitrogen dopant (b) as a function of the tip−sample separation. Tip−sample distance decreases from left to right. Red and blue dots point to the position of the boron and nitrogen atoms, respectively. In the experiment, the closest tip−sample separation $z_{rel.}$ = 0 corresponds to a tip approach of 150 pm from the STM point (−500 mV, 50 pA).

We performed AFM simulations[43] using the optimized atomic structure and Hartree potential of boron- and nitrogen-doped graphene obtained from total energy DFT calculations (see Methods for more details and Figure 3c for visualization of the Hartree potential). The simulated AFM images are in excellent agreement with the experimental observations and fully capture the contrast of the C−B and C−N bonds (Figure 2) as a function of the tip−sample separation. The optimized structure has negligible out-of-plane relaxation of the dopant, which allows us to exclude any role of topographic effects in the AFM contrast. To understand the origin of the contrast difference between boron and nitrogen dopants, the mechanism of high-resolution imaging has to be considered.[43,52,53] The CO-tip brought in the vicinity of the sample is sensitive to the total charge density distribution within the inspected system, and its variation can significantly affect the contrast. Intuitively, one can simplify the complex CO-tip charge distribution as a negatively effective charged tip. Thus, when probing an inhomogeneous charge distribution, the tip is repelled (less negative frequency shift) from sites of excess electron density, whereas it is attracted (more negative frequency shift) to those which have a positive charge. Therefore, the apparent contrast in the AFM images shows a substantial modification of the charge density localized at the C−B and C−N bonds.

Charge Distribution at Dopant Sites. This notion is substantiated by our KPFM measurements, also performed with a CO-tip. Figure 3a displays Kelvin parabolas, $\Delta f(V, z_{const.})$, acquired at a constant height over boron (red), nitrogen (blue), and carbon (yellow) atoms. We observe a strong variation of the local potential difference (LCPD) measured above the dopant atoms, compared to carbon atoms

https://dx.doi.org/10.1021/acssuschemeng.9b07623
ACS Sustainable Chem. Eng. 2020, 8, 3437−3444

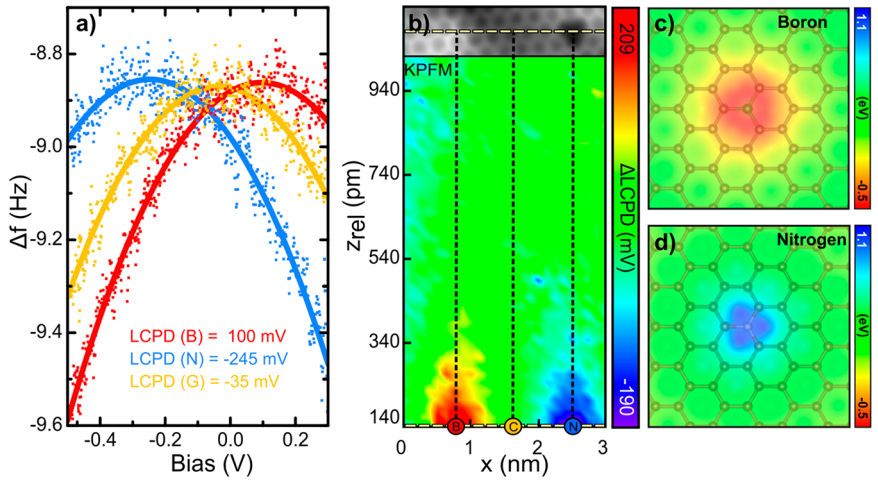

Figure 3. Net charge at the dopant sites in graphene. (a) KPFM parabolas above boron (red), carbon (yellow), and nitrogen (blue) atoms at the same tip−sample distance. KPFM plots are fitted with a parabolic dependence to obtain the LCPD value. (b) LCPD *x*-*z* map at different tip−sample separations *z* along a line crossing boron and nitrogen atoms (yellow dashed line in the inset AFM image). Each pixel corresponds with the fitted LCPD value of the KPFM parabola acquired in every (*x*, *z*) position. Errors in LCPD fittings are about 1.5 mV. (c, d) Calculated Hartree potential of single boron- and nitrogen-dopants in graphene.

of graphene, which we attribute primarily to the interaction of the CO-tip with inhomogeneous charge distribution. The LCPD over the boron/nitrogen dopant is shifted to a higher/lower value reflecting a decrease/increase of the local work function, respectively, induced by variation of the surface dipole around the dopants.[54,55]

To probe the spatial distribution of the net charges around the dopants, we acquired $\Delta f(V, x, z)$ spectra at different tip−sample separations z in the plane perpendicular to graphene and along the line crossing boron and nitrogen dopants (top AFM image in Figure 3b). In a posterior analysis, for each $\Delta f(V)$ curve, we determined the LCPD values by fitting. To extract the local impact of the dopants with respect to pristine graphene, we intentionally subtract the background LCPD signal obtained on pristine graphene areas. After such processing, we plotted a LCPD difference *x*-*z* map with respect to graphene (ΔLCPD *x*-*z*). At tip−sample height $z_{rel.}$ = 140 pm, the boron and nitrogen atoms show almost equal magnitudes of ΔLCPD but with opposite signs (Figure 3b). The sign reflects localization of positive and negative net charges on nitrogen and boron sites, respectively. On the other hand, the similar magnitude indicates a comparable level of opposite charge doping by boron and nitrogen, in good agreement with previous observations.[2,3] Quantitatively, LCPD values crucially depend on the mesoscopic tip termination due to long-range electrostatic forces,[56] but in repeated experimental sessions, we observed similar qualitative LCPD as described above, i.e., equal but opposite values for nitrogen and boron with respect to graphene, since the shift is always determined by the direction of the dipole induced by the dopant.[57,58]

In addition, at the selected separations, a negligible charge redistribution or transfer is observed through the CO molecule−dopant contact (Figure S3). Thus, we unambiguously interpret the observed contrast as a variation of the work function in the vicinity of the dopants. The ΔLCPD value on both dopants decreases continuously upon tip separations larger than $z_{rel.}$ = 290 pm, where the average graphene work function prevails. The ΔLCPD *x*-*z* map shows the lateral and vertical confinement of a net positive/negative charge in a small volume centered on the dopant atom.

These experimental observations are fully supported by the total energy DFT calculations. The presence of a negative/positive net charge on boron/nitrogen dopants is evident from the calculated Hartree potential (Figure 3c,d). However, a quantitative agreement between KPFM experiments and theoretical analysis is still missing and beyond the scope of this study. These charges are localized at the atom sites and extend only a few angstroms into the graphene basal plane, which is fully consistent with the spatial confinement of the charge observed in the LCPD map. The net charge on the boron/nitrogen dopants originates from acceptance/donation of an electron to the graphene pi-band[32,59] and subsequent electronic redistribution.

Chemical Properties of Individual Dopants. Finally, we focus on the chemical properties of the dopants. The force interaction between the CO molecule attached to the AFM tip apex and the incorporated dopants is investigated by means of site-specific $\Delta f(z)$ spectroscopy. $\Delta f(z)$ values above nitrogen (blue) and boron (red) atoms are displayed in Figure 4a and b, respectively, in addition to a reference $\Delta f(z)$ above a nearby carbon atom (yellow). No significant difference between the dopants and the reference carbon is seen in the Δf at larger distances (z_{rel} > 250 pm). For smaller separations, a difference in Δf becomes apparent. This difference is the largest at the minima of Δf for each atom (z_{rel} about 75 pm). Qualitatively, we found that the minimum Δf on nitrogen shows a more negative frequency shift, followed by carbon and boron atoms. At closer separations where Pauli repulsion starts affecting the total interaction, the Δf measured on dopants converges to that of nearby carbon, due to the interplay of electrostatic interaction and Pauli repulsion plus the different van der Waals radii of the atoms.[51] The $\Delta f(z)$ spectroscopy fully agrees with the observed atomic-scale contrast on dopants shown in Figure 2.

We quantify the effect of doping on graphene chemical properties by calculating the forces from the experimental $\Delta f(z)$ plot.[60] Dopant-independent force components were removed by subtraction of the $\Delta f(z)$ measured on top of a

https://dx.doi.org/10.1021/acssuschemeng.9b07623
ACS Sustainable Chem. Eng. 2020, 8, 3437−3444

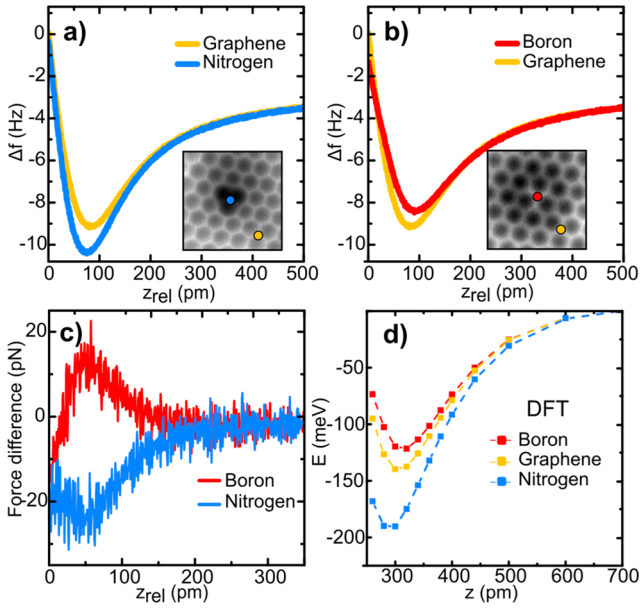

Figure 4. Quantification of interaction of graphene dopants with CO molecule. (a, b) Site-specific $\Delta f(z)$ plots on nitrogen (blue), boron (red), and carbon (yellow) atoms with a CO-tip. Colored circles indicate the exact site of acquisition in the corresponding AFM images in the insets. (c) Force difference between the CO-tip and the boron (red) and nitrogen dopants (blue), with the CO-carbon reference subtracted. (d) DFT-calculated interaction energies between a CO-tip and nitrogen (blue), boron (red), and carbon (yellow) atoms in graphene. Here, the z coordinate indicates the distance between the graphene layer and the oxygen atom in the CO-tip.

carbon atom before the calculation process. Figure 4c shows the force difference of nitrogen (blue line) and boron (red line) dopants with respect to carbon atoms, sensed by the CO-tip. We observe the augmented interaction of CO with graphitic nitrogen by approximately 25 pN. On the other hand, the interaction of CO with the boron dopant is reduced by approximately 15 pN. Despite these rather small force differences, AFM with a CO-tip demonstrates being a technique sensitive enough to visualize single dopants in graphene and their chemical activity.

This observation is in line with DFT+vdW calculations of the tip−graphene interaction. We mimic the experimental setup by the Au(111)-CO pyramidal-tip above a 5 × 5 graphene lattice in which single nitrogen and boron atoms are localized at graphitic sites. Figure 4d displays the vertical component for the calculated tip−sample interaction energy which reproduces the experimental findings. The calculation yields the highest interaction energy for the CO-tip above the nitrogen atom ($E_N \approx 190$ meV) followed by the carbon atom ($E_C \approx 140$ meV) and the boron atom ($E_B \approx 120$ meV). Note that the tip−graphene system is allowed to fully relax; i.e., only the last plane of the tip Au atoms and carbon atoms distant from the tip are fixed during the calculation. The exact value of the calculated interaction energy is quantitatively sensitive to the choice of the functional used for a description of the van der Waals interaction, which is not covered by standard exchange−correlation functionals as a generalized gradient approximation (GGA). Nevertheless, the order $E_N > E_C > E_B$ and energetic difference between the atoms remain the same for various inspected functionals (see Figure S2 and Methods for more details). Moreover, the calculation shows that the van der Waals interaction is very uniform above the doped graphene. The differences in the interaction are thus governed by electrostatic forces between the tip and charge density localized around the respective atomic site.

CONCLUSIONS

In summary, we have investigated the physicochemical properties of single substitutional N and B dopants in a graphene monolayer at the atomic-scale by means of combined AFM and KPFM measurements corroborated with DFT simulations. The very good agreement of our theoretical calculations with the experimental findings provides a detailed understanding of the local charge distribution of single dopants. We evaluated the weak chemical interactions of nitrogen and boron dopants with single CO molecules attached to the tip-apex by means of experimental measurements of site-specific force spectroscopy and DFT calculations. Our results demonstrate the divergent chemical activity of nitrogen and boron impurities incorporated into graphene and provide a deeper insight for a precise chemical functionalization of graphene derivatives.

ASSOCIATED CONTENT

Supporting Information

The Supporting Information is available free of charge at https://pubs.acs.org/doi/10.1021/acssuschemeng.9b07623.

Figure S1: Moiré corrugation estimation. Figure S2: Comparison of interaction energy and force for different vdW functional. Figure S3: Analysis of the charge redistribution in the CO−dopant junction. Figure S4: Analysis of bond distortion. Figure S5: AFM with metallic tip. (PDF)

AUTHOR INFORMATION

Corresponding Authors

Pavel Jelínek − *Regional Centre of Advanced Technologies and Materials, Faculty of Science, Palacký University Olomouc, 78371 Olomouc, Czech Republic; Institute of Physics, Czech Academy of Sciences, 16200 Prague, Czech Republic;* orcid.org/0000-0002-5645-8542; Email: jelinekp@fzu.cz

Martin Švec − *Regional Centre of Advanced Technologies and Materials, Faculty of Science, Palacký University Olomouc, 78371 Olomouc, Czech Republic; Institute of Physics, Czech Academy of Sciences, 16200 Prague, Czech Republic;* Email: svec@fzu.cz

Bruno de la Torre − *Regional Centre of Advanced Technologies and Materials, Faculty of Science, Palacký University Olomouc, 78371 Olomouc, Czech Republic; Institute of Physics, Czech Academy of Sciences, 16200 Prague, Czech Republic;* orcid.org/0000-0002-6462-6833; Email: bdelatorre@fzu.cz

Authors

Benjamin Mallada − *Regional Centre of Advanced Technologies and Materials, Faculty of Science, Palacký University Olomouc, 78371 Olomouc, Czech Republic; Institute of Physics, Czech Academy of Sciences, 16200 Prague, Czech Republic;* orcid.org/0000-0002-8209-9977

Shayan Edalatmanesh − *Regional Centre of Advanced Technologies and Materials, Faculty of Science, Palacký University Olomouc, 78371 Olomouc, Czech Republic*

https://dx.doi.org/10.1021/acssuschemeng.9b07623
ACS Sustainable Chem. Eng. 2020, 8, 3437−3444

Petr Lazar − *Regional Centre of Advanced Technologies and Materials, Faculty of Science, Palacký University Olomouc, 78371 Olomouc, Czech Republic;* orcid.org/0000-0002-7312-3656

Jesus Redondo − *Institute of Physics, Czech Academy of Sciences, 16200 Prague, Czech Republic; Faculty of Mathematics and Physics, Charles University, 180 00 Prague, Czech Republic;* orcid.org/0000-0002-8147-689X

Aurelio Gallardo − *Institute of Physics, Czech Academy of Sciences, 16200 Prague, Czech Republic; Faculty of Mathematics and Physics, Charles University, 180 00 Prague, Czech Republic;* orcid.org/0000-0001-6544-7637

Radek Zbořil − *Regional Centre of Advanced Technologies and Materials, Faculty of Science, Palacký University Olomouc, 78371 Olomouc, Czech Republic; Institute of Organic Chemistry and Biochemistry, Czech Academy of Sciences, 16610 Prague 6, Czech Republic;* orcid.org/0000-0002-3147-2196

Complete contact information is available at: https://pubs.acs.org/10.1021/acssuschemeng.9b07623

Author Contributions

The manuscript was written through contributions of all authors. All authors have given approval to the final version of the manuscript.

Notes

The authors declare no competing financial interest.

■ ACKNOWLEDGMENTS

Work was supported by GACR 18-09914S and Operational Programme Research, Development and Education financed by the European Structural and Investment Funds and the Czech Ministry of Education, Youth and Sports (Project No. CZ.02.1.01/0.0/0.0/16_019/0000754). P.J. acknowledges support from the Praemium Academie of the Academy of Science of the Czech Republic. The authors gratefully acknowledge the support from the EXPRO 19-27454X project from the Czech Science Foundation (GA-CR). M.Š. acknowledges the support of the Czech Grant Agency No. 17-24210Y.

■ REFERENCES

(1) Schiros, T.; Nordlund, D.; Palova, L.; Zhao, L.; Levendorf, M.; Jaye, C.; Reichman, D.; Park, J.; Hybertsen, M.; Pasupathy, A. Atomistic Interrogation of B−N Co-Dopant Structures and Their Electronic Effects in Graphene. *ACS Nano* **2016**, *10* (7), 6574−6584.

(2) Zhao, L.; He, R.; Rim, K. T.; Schiros, T.; Kim, K. S.; Zhou, H.; Gutierrez, C.; Chockalingam, S. P.; Arguello, C. J.; Palova, L.; et al. Visualizing Individual Nitrogen Dopants in MonolayerGraphene. *Science* **2011**, *333* (6045), 999−1003.

(3) Zhao, L.; Levendorf, M.; Goncher, S.; Schiros, T.; Pálová, L.; Zabet-Khosousi, A.; Rim, K. T.; Gutiérrez, C.; Nordlund, D.; Jaye, C.; et al. Local Atomic and Electronic Structure of Boron Chemical Doping in Monolayer Graphene. *Nano Lett.* **2013**, *13* (10), 4659−4665.

(4) Telychko, M.; Mutombo, P.; Merino, P.; Hapala, P.; Ondráček, M.; Bocquet, F. C.; Sforzini, J.; Stetsovych, O.; Vondráček, M.; Jelínek, P.; et al. Electronic and Chemical Properties of Donor, Acceptor Centers in Graphene. *ACS Nano* **2015**, *9* (9), 9180−9187.

(5) Li, J.; Lin, L.; Rui, D.; Li, Q.; Zhang, J.; Kang, N.; Zhang, Y.; Peng, H.; Liu, Z.; Xu, H. Q. Electron−Hole Symmetry Breaking in Charge Transport in Nitrogen-Doped Graphene. *ACS Nano* **2017**, *11* (5), 4641−4650.

(6) Nigar, S.; Zhou, Z.; Wang, H.; Imtiaz, M. Modulating the Electronic and Magnetic Properties of Graphene. *RSC Adv.* **2017**, *7* (81), 51546−51580.

(7) Hage, F. S.; Hardcastle, T. P.; Gjerding, M. N.; Kepaptsoglou, D. M.; Seabourne, C. R.; Winther, K. T.; Zan, R.; Amani, J. A.; Hofsaess, H. C.; Bangert, U.; et al. Local Plasmon Engineering in Doped Graphene. *ACS Nano* **2018**, *12* (2), 1837−1848.

(8) Błoński, P.; Tuček, J.; Sofer, Z.; Mazánek, V.; Petr, M.; Pumera, M.; Otyepka, M.; Zbořil, R. Doping with Graphitic Nitrogen Triggers Ferromagnetism in Graphene. *J. Am. Chem. Soc.* **2017**, *139* (8), 3171−3180.

(9) Georgakilas, V.; Tiwari, J. N.; Kemp, K. C.; Perman, J. A.; Bourlinos, A. B.; Kim, K. S.; Zboril, R. Noncovalent Functionalization of Graphene and Graphene Oxide for Energy Materials, Biosensing, Catalytic, and Biomedical Applications. *Chem. Rev.* **2016**, *116* (9), 5464−5519.

(10) Kuila, T.; Bose, S.; Mishra, A. K.; Khanra, P.; Kim, N. H.; Lee, J. H. Chemical Functionalization of Graphene and Its Applications. *Prog. Mater. Sci.* **2012**, *57* (7), 1061−1105.

(11) Wang, H.; Maiyalagan, T.; Wang, X. Review on Recent Progress in Nitrogen-Doped Graphene: Synthesis, Characterization, and Its Potential Applications. *ACS Catal.* **2012**, *2* (5), 781−794.

(12) Agnoli, S.; Favaro, M. Doping Graphene with Boron: A Review of Synthesis Methods, Physicochemical Characterization, and Emerging Applications. *J. Mater. Chem. A* **2016**, *4* (14), 5002−5025.

(13) Lazar, P.; Zbořil, R.; Pumera, M.; Otyepka, M. Chemical Nature of Boron and Nitrogen Dopant Atoms in Graphene Strongly Influences Its Electronic Properties. *Phys. Chem. Chem. Phys.* **2014**, *16* (27), 14231−14235.

(14) Panchakarla, L. S.; Subrahmanyam, K. S.; Saha, S. K.; Govindaraj, A.; Krishnamurthy, H. R.; Waghmare, U. V.; Rao, C. N. R. Synthesis, Structure, and Properties of Boron- and Nitrogen-Doped Graphene. *Adv. Mater.* **2009**, *21* (46), 4726−4730.

(15) Zheng, Y.; Jiao, Y.; Ge, L.; Jaroniec, M.; Qiao, S. Z. Two-Step Boron and Nitrogen Doping in Graphene for Enhanced Synergistic Catalysis. *Angew. Chem., Int. Ed.* **2013**, *52* (11), 3110−3116.

(16) Rao, C. N. R.; Gopalakrishnan, K.; Govindaraj, A. Synthesis, Properties and Applications of Graphene Doped with Boron, Nitrogen and Other Elements. *Nano Today* **2014**, *9* (3), 324−343.

(17) Usachov, D.; Vilkov, O.; Gruneis, A.; Haberer, D.; Fedorov, A.; Adamchuk, V. K.; Preobrajenski, A. B.; Dudin, P.; Barinov, A.; Oehzelt, M.; Laubschat, C.; Vyalikh, D. V. Nitrogen-Doped Graphene: Efficient Growth, Structure, and Electronic Properties. *Nano Lett.* **2011**, *11* (12), 5401−5407.

(18) Velez-Fort, E.; Mathieu, C.; Pallecchi, E.; Pigneur, M.; Silly, M. G.; Belkhou, R.; Marangolo, M.; Shukla, A.; Sirotti, F.; Ouerghi, A. Epitaxial Graphene on 4H-SiC(0001) Grown under Nitrogen Flux: Evidence of Low Nitrogen Doping and High Charge Transfer. *ACS Nano* **2012**, *6* (12), 10893−10900.

(19) Joucken, F.; Tison, Y.; Lagoute, J.; Dumont, J.; Cabosart, D.; Zheng, B.; Repain, V.; Chacon, C.; Girard, Y.; Botello-Mendez, A. R.; Rousset, S.; Sporken, R.; Charlier, J. C.; Henrard, L. Localized state and charge transfer in nitrogen-doped graphene. *Phys. Rev. B: Condens. Matter Mater. Phys.* **2012**, *85* (16), 161408.

(20) Schiros, T.; Nordlund, D.; Palova, L.; Prezzi, D.; Zhao, L. Y.; Kim, K. S.; Wurstbauer, U.; Gutierrez, C.; Delongchamp, D.; Jaye, C.; Fischer, D.; Ogasawara, H.; Pettersson, L. G. M.; Reichman, D. R.; Kim, P.; Hybertsen, M. S.; Pasupathy, A. N. Connecting Dopant Bond Type with Electronic Structure in N-Doped Graphene. *Nano Lett.* **2012**, *12* (8), 4025−4031.

(21) Wood, K. N.; Christensen, S. T.; Nordlund, D.; Dameron, A. A.; Ngo, C.; Dinh, H.; Gennett, T.; O'Hayre, R.; Pylypenko, S. Spectroscopic investigation of nitrogen-functionalized carbon materials. *Surf. Interface Anal.* **2016**, *48* (5), 283−292.

(22) Muhich, C. L.; Westcott, J. Y.; Morris, T. C.; Weimer, A. W.; Musgrave, C. B. The Effect of N and B Doping on Graphene and the Adsorption and Migration Behavior of Pt Atoms. *J. Phys. Chem. C* **2013**, *117* (20), 10523−10535.

(23) Zhang, L. P.; Xia, Z. H. Mechanisms of Oxygen Reduction Reaction on Nitrogen-Doped Graphene for Fuel Cells. *J. Phys. Chem. C* **2011**, *115* (22), 11170−11176.
(24) Zhang, L. P.; Niu, J. B.; Dai, L.; Xia, Z. H. Effect of Microstructure of Nitrogen-Doped Graphene on Oxygen Reduction Activity in Fuel Cells. *Langmuir* **2012**, *28* (19), 7542−7550.
(25) Marconcini, P.; Cresti, A.; Triozon, F.; Fiori, G.; Biel, B.; Niquet, Y. M.; Macucci, M.; Roche, S. Atomistic Boron-Doped Graphene Field-Effect Transistors: A Route toward Unipolar Characteristics. *ACS Nano* **2012**, *6* (9), 7942−7947.
(26) Lherbier, A.; Botello-Mendez, A. R.; Charlier, J. C. Electronic and Transport Properties of Unbalanced Sublattice N-Doping in Graphene. *Nano Lett.* **2013**, *13* (4), 1446−1450.
(27) Kong, X. K.; Chen, C. L.; Chen, Q. W. Doped graphene for metal-free catalysis. *Chem. Soc. Rev.* **2014**, *43* (8), 2841−2857.
(28) Georgakilas, V.; Otyepka, M.; Bourlinos, A. B.; Chandra, V.; Kim, N.; Kemp, K. C.; Hobza, P.; Zboril, R.; Kim, K. S. Functionalization of Graphene: Covalent and Non-Covalent Approaches, Derivatives and Applications. *Chem. Rev.* **2012**, *112* (11), 6156−6214.
(29) de la Torre, B.; Svec, M.; Hapala, P.; Redondo, J.; Krejci, O.; Lo, R.; Manna, D.; Sarmah, A.; Nachtigallova, D.; Tucek, J.; Blonski, P.; Otyepka, M.; Zboril, R.; Hobza, P.; Jelinek, P. Non-covalent control of spin-state in metal-organic complex by positioning on N-doped graphene. *Nat. Commun.* **2018**, *9*, 2831.
(30) Pham, V. D.; Lagoute, J.; Mouhoub, O.; Joucken, F.; Repain, V.; Chacon, C.; Bellec, A.; Girard, Y.; Rousset, S. Electronic Interaction between Nitrogen-Doped Graphene and Porphyrin Molecules. *ACS Nano* **2014**, *8* (9), 9403−9409.
(31) Gross, L.; Mohn, F.; Moll, N.; Liljeroth, P.; Meyer, G. The Chemical Structure of a Molecule Resolved by Atomic Force Microscopy. *Science* **2009**, *325* (5944), 1110−1114.
(32) Sforzini, J.; Telychko, M.; Krejci, O.; Vondracek, M.; Svec, M.; Bocquet, F. C.; Tautz, F. S. Transformation of metallic boron into substitutional dopants in graphene on 6*H*-SiC(0001). *Phys. Rev. B: Condens. Matter Mater. Phys.* **2016**, *93* (4), 041302.
(33) Horcas, I.; Fernandez, R.; Gomez-Rodriguez, J. M.; Colchero, J.; Gomez-Herrero, J.; Baro, A. M. WSXM: A software for scanning probe microscopy and a tool for nanotechnology. *Rev. Sci. Instrum.* **2007**, *78* (1), 013705.
(34) Blochl, P. E. Projector Augmented-Wave Method. *Phys. Rev. B: Condens. Matter Mater. Phys.* **1994**, *50* (24), 17953−17979.
(35) Kresse, G.; Joubert, D. From ultrasoft pseudopotentials to the projector augmented-wave method. *Phys. Rev. B: Condens. Matter Mater. Phys.* **1999**, *59* (3), 1758−1775.
(36) Klimes, J.; Bowler, D. R.; Michaelides, A. Van der Waals density functionals applied to solids. *Phys. Rev. B: Condens. Matter Mater. Phys.* **2011**, *83* (19), 195131.
(37) Lazar, P.; Karlicky, F.; Jurecka, P.; Kocman, M.; Otyepkova, E.; Safarova, K.; Otyepka, M. Adsorption of Small Organic Molecules on Graphene. *J. Am. Chem. Soc.* **2013**, *135* (16), 6372−6377.
(38) Lazar, P.; Martincova, J.; Otyepka, M. Structure, dynamical stability, and electronic properties of phases in TaS_2 from a high-level quantum mechanical calculation. *Phys. Rev. B: Condens. Matter Mater. Phys.* **2015**, *92* (22), 224104.
(39) Tkatchenko, A.; DiStasio, R. A.; Car, R.; Scheffler, M. Accurate and Efficient Method for Many-Body van Der Waals Interactions. *Phys. Rev. Lett.* **2012**, *108* (23), 236402.
(40) Momma, K.; Izumi, F. VESTA 3 for three-dimensional visualization of crystal, volumetric and morphology data. *J. Appl. Crystallogr.* **2011**, *44*, 1272−1276.
(41) Blum, V.; Gehrke, R.; Hanke, F.; Havu, P.; Havu, V.; Ren, X.; Reuter, K.; Scheffler, M. Ab Initio Molecular Simulations with Numeric Atom-Centered Orbitals. *Comput. Phys. Commun.* **2009**, *180* (11), 2175−2196.
(42) Perdew, J. P.; Burke, K.; Ernzerhof, M. Generalized Gradient Approximation Made Simple. *Phys. Rev. Lett.* **1996**, *77* (18), 3865−3868.
(43) Hapala, P.; Kichin, G.; Wagner, C.; Tautz, F. S.; Temirov, R.; Jelinek, P. Mechanism of high-resolution STM/AFM imaging with functionalized tips. *Phys. Rev. B: Condens. Matter Mater. Phys.* **2014**, *90* (8), 085421.
(44) Peng, J.; Guo, J.; Hapala, P.; Cao, D.; Ma, R.; Cheng, B.; Xu, L.; Ondráček, M.; Jelínek, P.; Wang, E.; et al. Weakly Perturbative Imaging of Interfacial Water with Submolecular Resolution by Atomic Force Microscopy. *Nat. Commun.* **2018**, *9* (1), 2831.
(45) Martin-Recio, A.; Romero-Muniz, C.; Pou, P.; Perez, R.; Gomez-Rodriguez, J. M. Purely substitutional nitrogen on graphene/Pt(111) unveiled by STM and first principles calculations. *Nanoscale* **2016**, *8* (40), 17686−17693.
(46) de la Torre, B.; Ellner, M.; Pou, P.; Nicoara, N.; Perez, R.; Gomez-Rodriguez, J. M. Atomic-Scale Variations of the Mechanical Response of 2D Materials Detected by Noncontact Atomic Force Microscopy. *Phys. Rev. Lett.* **2016**, *116* (24), 245502.
(47) Boneschanscher, M. P.; van der Lit, J.; Sun, Z. X.; Swart, I.; Liljeroth, P.; Vanmaekelbergh, D. Quantitative Atomic Resolution Force Imaging on Epitaxial Graphene with Reactive and Nonreactive AFM Probes. *ACS Nano* **2012**, *6* (11), 10216−10221.
(48) Schwarz, M.; Riss, A.; Garnica, M.; Ducke, J.; Deimel, P. S.; Duncan, D. A.; Thakur, P. K.; Lee, T. L.; Seitsonen, A. P.; Barth, J. V.; Allegretti, F.; Auwarter, W. Corrugation in the Weakly Interacting Hexagonal-BN/Cu(111) System: Structure Determination by Combining Noncontact Atomic Force Microscopy and X-ray Standing Waves. *ACS Nano* **2017**, *11* (9), 9151−9161.
(49) Telychko, M.; Berger, J.; Majzik, Z.; Jelinek, P.; Svec, M. Graphene on SiC(0001) inspected by dynamic atomic force microscopy at room temperature. *Beilstein J. Nanotechnol.* **2015**, *6*, 901−906.
(50) Hapala, P.; Svec, M.; Stetsovych, O.; van der Heijden, N. J.; Ondracek, M.; van der Lit, J.; Mutombo, P.; Swart, I.; Jelinek, P. Mapping the electrostatic force field of single molecules from high-resolution scanning probe images. *Nat. Commun.* **2016**, *7* (1), 11560.
(51) Kawai, S.; Nakatsuka, S.; Hatakeyama, T.; Pawlak, R.; Meier, T.; Tracey, J.; Meyer, E.; Foster, A. S. Multiple heteroatom substitution to graphene nanoribbon. *Sci. Adv.* **2018**, *4* (4), eaar7181.
(52) Moll, N.; Gross, L.; Mohn, F.; Curioni, A.; Meyer, G. The mechanisms underlying the enhanced resolution of atomic force microscopy with functionalized tips. *New J. Phys.* **2010**, *12*, 125020.
(53) Ellner, M.; Pavlicek, N.; Pou, P.; Schuler, B.; Moll, N.; Meyer, G.; Gross, L.; Perez, R. The Electric Field of CO Tips and Its Relevance for Atomic Force Microscopy. *Nano Lett.* **2016**, *16* (3), 1974−1980.
(54) Mohn, F.; Gross, L.; Moll, N.; Meyer, G. Imaging the charge distribution within a single molecule. *Nat. Nanotechnol.* **2012**, *7* (4), 227−231.
(55) Gross, L.; Mohn, F.; Liljeroth, P.; Repp, J.; Giessibl, F. J.; Meyer, G. Measuring the Charge State of an Adatom with Noncontact Atomic Force Microscopy. *Science* **2009**, *324* (5933), 1428−1431.
(56) Bocquet, F.; Nony, L.; Loppacher, C. Polarization effects in noncontact atomic force microscopy: A key to model the tip-sample interaction above charged adatoms. *Phys. Rev. B: Condens. Matter Mater. Phys.* **2011**, *83* (3), 035411.
(57) Albrecht, F.; Repp, J.; Fleischmann, M.; Scheer, M.; Ondracek, M.; Jelinek, P. Probing Charges on the Atomic Scale by Means of Atomic Microscopy. *Phys. Rev. Lett.* **2015**, *115* (7), 076101.
(58) Gross, L.; Schuler, B.; Mohn, F.; Moll, N.; Pavlicek, N.; Steurer, W.; Scivetti, I.; Kotsis, K.; Persson, M.; Meyer, G. Investigating atomic contrast in atomic force microscopy and Kelvin probe force microscopy on ionic systems using functionalized tips. *Phys. Rev. B: Condens. Matter Mater. Phys.* **2014**, *90* (15), 155455.
(59) Sforzini, J.; Hapala, P.; Franke, M.; van Straaten, G.; Stohr, A.; Link, S.; Soubatch, S.; Jelinek, P.; Lee, T. L.; Starke, U.; Svec, M.; Bocquet, F. C.; Tautz, F. S. Structural and Electronic Properties of Nitrogen-Doped Graphene. *Phys. Rev. Lett.* **2016**, *116* (12), 126805.

https://dx.doi.org/10.1021/acssuschemeng.9b07623
ACS Sustainable Chem. Eng. 2020, 8, 3437−3444

(60) Giessibl, F. J. A direct method to calculate tip-sample forces from frequency shifts in frequency-modulation atomic force microscopy. *Appl. Phys. Lett.* **2001**, *78* (1), 123−125.

https://dx.doi.org/10.1021/acssuschemeng.9b07623
ACS Sustainable Chem. Eng. 2020, 8, 3437−3444